



Methylene-tetrahydrofolate reductase (MTHFR)



A Target Enabling Package (TEP)

Gene ID / UniProt ID / EC	4524 / P42898 / EC 1.5.1.20
Target Nominator	D. Sean Froese ¹ , Matthias Baumgartner ¹
SGC Authors	Jola Kopec, Gustavo A. Bezerra, Rod Chalk, Elzbieta Rembeza, William R. Foster, Oktawia Borkowska, Peter J. Brown
Collaborating Authors	D. Sean Froese ¹ , Terttu Suormala ¹ , Seraina Lutz ¹ , Matthias Baumgartner ¹ , Kevin G. Hicks ² , Jared Rutter ² , Minkui Luo ³
Target PI	Wyatt W. Yue (SGC Oxford)
Therapeutic Area(s)	Metabolic disorders, cancer
Disease Relevance	Autosomal recessive mutations cause MTHFR deficiency (OMIM 236250); common genetic variants are associated with ischemic stroke (OMIM 601367), folate-sensitive neural tube defects (OMIM 601634) and schizophrenia (OMIM 181500)
Date Approved by TEP Evaluation Group	9/12/2019
Document version	Version 3
Document version date	October 2020
Citation	10.5281/zenodo.3584528
Affiliations	¹ Division of Metabolism and Children's Research Center, University Children's Hospital, Zürich; ² Department of Biochemistry, University of Utah School of Medicine; ³ Memorial Sloan Kettering Cancer Center, New York.

USEFUL LINKS



(Please note that the inclusion of links to external sites should not be taken as an endorsement of that site by the SGC in any way)

SUMMARY OF PROJECT

The folate and methionine cycles are essential metabolic pathways for life, involved respectively in DNA synthesis and generation of the ubiquitous methyl donor S-adenosylmethionine (SAM). The enzyme 5,10-methylenetetrahydrofolate reductase (MTHFR) represents a key regulatory connection between these cycles, hence exerting a strong influence on an array of diseases. This TEP presents the first structures for any eukaryotic MTHFR, revealing a novel SAM-binding fold. The TEP applies mass spectrometry, activity assay and biophysical binding methods to determine how phosphorylation and allosteric binding of SAM act in concert to inhibit MTHFR activity. This work also provides the starting point for the design of tool molecules (e.g. SAM-analogues) aimed at modulating the SAM-induced inhibition of MTHFR activity.

SCIENTIFIC BACKGROUND

The enzyme 5,10-methylenetetrahydrofolate reductase (MTHFR) is situated at the intersection between the *folate cycle* required for purine and thymidylate synthesis, and the *methionine cycle* responsible for synthesis of the ubiquitous methyl donor *s*-adenosylmethionine (AdoMet, or SAM)(1) (**Fig. 1**). Together, these two metabolic cycles regulate the flow of folate-mediated one-carbon units to drive essential processes for cell survival.

MTHFR catalyses the physiologically irreversible reduction of methylenetetrahydrofolate (CH₂-THF) to methyltetrahydrofolate (CH₃-THF), requiring FAD as cofactor and NADPH as electron donor. Since the product CH₃-THF is exclusively used in the methionine cycle (via methionine synthase, MTR), by carrying out this physiologically irreversible reaction MTHFR dedicates folate-mediated one-carbon units towards methionine and SAM synthesis.

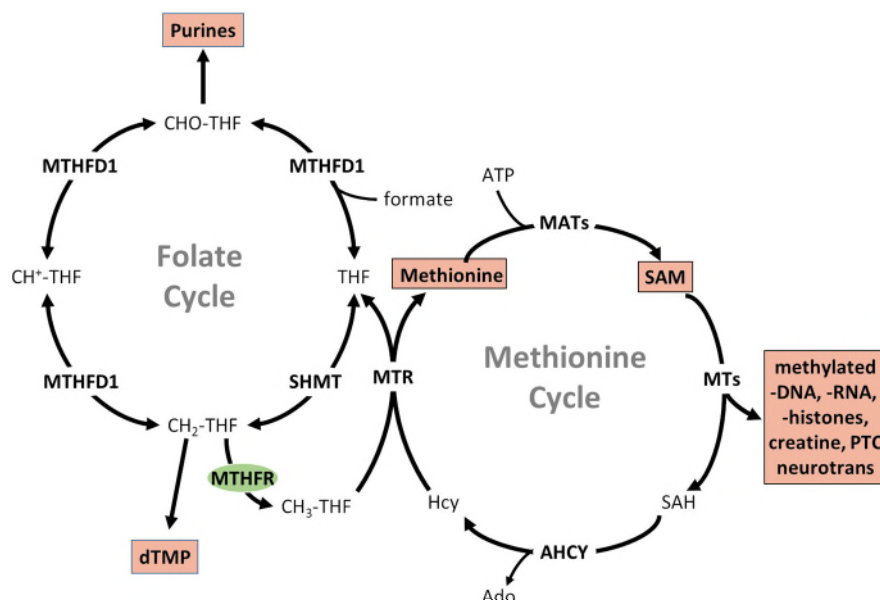


Fig. 1 MTHFR at the intersection of the folate cycle and methionine cycle in one-carbon metabolism.

In metazoans, MTHFR activity is regulated by the methionine cycle product SAM through allosteric inhibition (2), a process that is enhanced by its own phosphorylation (3-5) and reversed by its binding to *s*-adenosylhomocysteine (AdoHcy, or SAH), the de-methylated form of SAM (6). Neither of these inhibitory mechanisms have been understood to date in the absence of protein structural data.

Disease linkage:

- **Metabolic/rare disease/neuro-psychiatry:** MTHFR deficiency (MIM #236250) is an ultra-rare autosomal recessive disorder (with approximately 200 patients known) characterised by phenotypes ranging from neurological deterioration and early death to asymptomatic adults (7).
- **MTHFR polymorphism** (e.g. p.Ala222Val, c.665C>T) is identified as a risk factor for a plethora of multifactorial disorders, including vascular diseases, neurological diseases, various cancers, diabetes and pregnancy loss (8). The exact mechanistic contribution is currently unclear, but may be associated with reduced enzymatic activity and lower circulating folate concentrations (9,10).

Therapeutic application:

In MTHFR deficiency, the majority of patients harbour missense mutations which reduce, but do not ablate, residual enzymatic activity; whereby the amount of residual activity remaining correlates with disease severity (7,11). For these patients, increasing MTHFR activity, either by mutant protein stabilization or by activity dis-inhibition (e.g. by blocking SAM binding or targeting the kinase(s) responsible for phosphorylation) may lower disease burden.

Members of the folate cycle, including MTHFR, have increasingly become a therapeutic target in cancer (12,13), consistent with an increased utilization of one-carbon units during cancer metabolism. There are two opposing rationales for targeting MTHFR in cancer.

1) *MTHFR* is responsible for creation of CH_3 -THF, the main circulatory folate form and the form specifically imported by cancer cells. As such:

- *MTHFR* expression is significantly upregulated in prostate tumour tissues. Overexpression of *MTHFR* correlates with cancer recurrence and death in prostate cancer datasets (14).
- Antisense inhibition of *MTHFR* reduces growth of human colon, lung, breast, prostate and neuroblastoma cell lines *in vitro*. *In vivo*, it inhibits growth of human colon and lung carcinoma xenografts (15,16).
- In mouse model of intestinal adenomas, low dietary folate and *MTHFR* deficiency reduce adenoma formation (17).

2) By creating CH_3 -THF, *MTHFR* shunts folates away from DNA synthesis and towards production of SAM, which is required for proper DNA methylation. As such:

- Reduced activity of *MTHFR* (p.Ala22Val) is associated with an increased risk of breast cancer (18)
- Changes in intracellular methionine levels lead to rapid changes in DNA methylation (19)
- Disruption of the methionine cycle results in altered DNA methylation in tumours and reduced survival (20)

Therefore, titratable disruption of *MTHFR* activity, either by enhancing inhibition e.g. via SAM analogues or active-site inhibitors, or by reducing inhibition e.g. by blocking SAM binding (e.g. through an SAH analogue) or by targeting the kinase(s) responsible for protein phosphorylation, may provide a means by which *MTHFR* activity and thus cancer appearance and progression may be controlled.

RESULTS – THE TEP

Proteins Purified

Human *MTHFR* adopts a multi-domain organisation (**Fig. 2**), whereby the core catalytic domain utilises FAD and NADPH as electron donors for catalysis, which is allosterically inhibited by binding of SAM to the C-terminal regulatory domain, a process sensitive to multiple phosphorylation at the far N-terminus.

- Using baculovirus-mediated insect cell expression, we expressed full-length human *MTHFR* (residues 1-656, hsMTHFR₁₋₆₅₆), and a near-full-length protein truncated at both termini (residues 38-644, hsMTHFR₃₈₋₆₄₄).
- We have also expressed in *E. coli* the human *MTHFR* regulatory domain (hsMTHFR₃₄₈₋₆₅₆).
- In addition to human *MTHFR*, we have generated recombinant soluble constructs (full-length protein and domains) for two orthologues from *Mus musculus* and *Saccharomyces cerevisiae*.

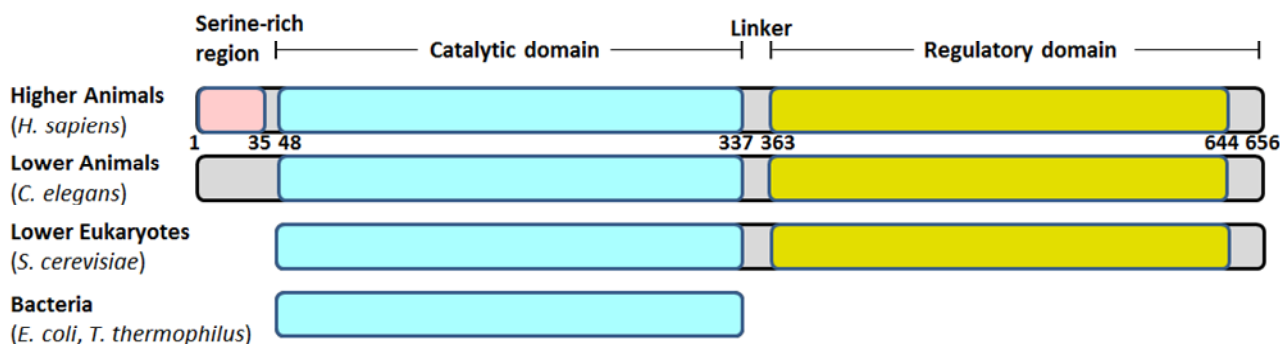


Fig. 2 Domain organisation of *MTHFR* orthologues across evolution.

In Vitro Assays

Mass spectrometry

Human MTHFR contains an N-terminal 35-residue serine-rich region not found in orthologues of bacteria, yeast or even lower animals. We have performed mass spectrometry-based phosphorylation mapping of hsMTHFR₁₋₆₅₆ (with 92% coverage) and identified 11 phosphorylation sites within this region (Ser9, Ser10, Ser18, Ser20, Ser21, Ser23, Ser25, Ser26, Ser29, Ser30, Thr34). As expected, hsMTHFR₃₈₋₆₄₄, which lacks this N-terminal region, was not found to be phosphorylated.

Activity assay

Our collaborators in Zürich have developed a novel HPLC-based activity assay to probe the complete enzymatic reaction in the physiological direction (21). This assay allows separation and quantitation of the product CH₃-THF from substrate CH₂-THF and hence the determination of full kinetic values including specific activity, K_M , and K_i (for SAM). This assay is compatible with purified protein, endogenous protein from cellular lysates (including patient fibroblasts), and over-expressed protein from cellular lysates (any organism). Comparison between hsMTHFR₁₋₆₅₆ and hsMTHFR₃₈₋₆₄₄ does not reveal significant changes in kinetic properties attributable to N-terminal phosphorylation.

Using this assay, we have confirmed the role of SAM as an inhibitor of MTHFR enzymatic activity exhibiting an inhibition constant (K_i) of $\sim 3 \mu\text{M}$ for hsMTHFR₁₋₆₅₆ protein. Dephosphorylated hsMTHFR₁₋₆₅₆ and phosphorylation-deficient hsMTHFR₃₈₋₆₄₄ have 2-fold and 7-fold higher K_i for SAM, respectively (Fig. 3a). Thus, whilst phosphorylation does not directly affect MTHFR enzymatic activity, it increases the protein's sensitivity to SAM inhibition.

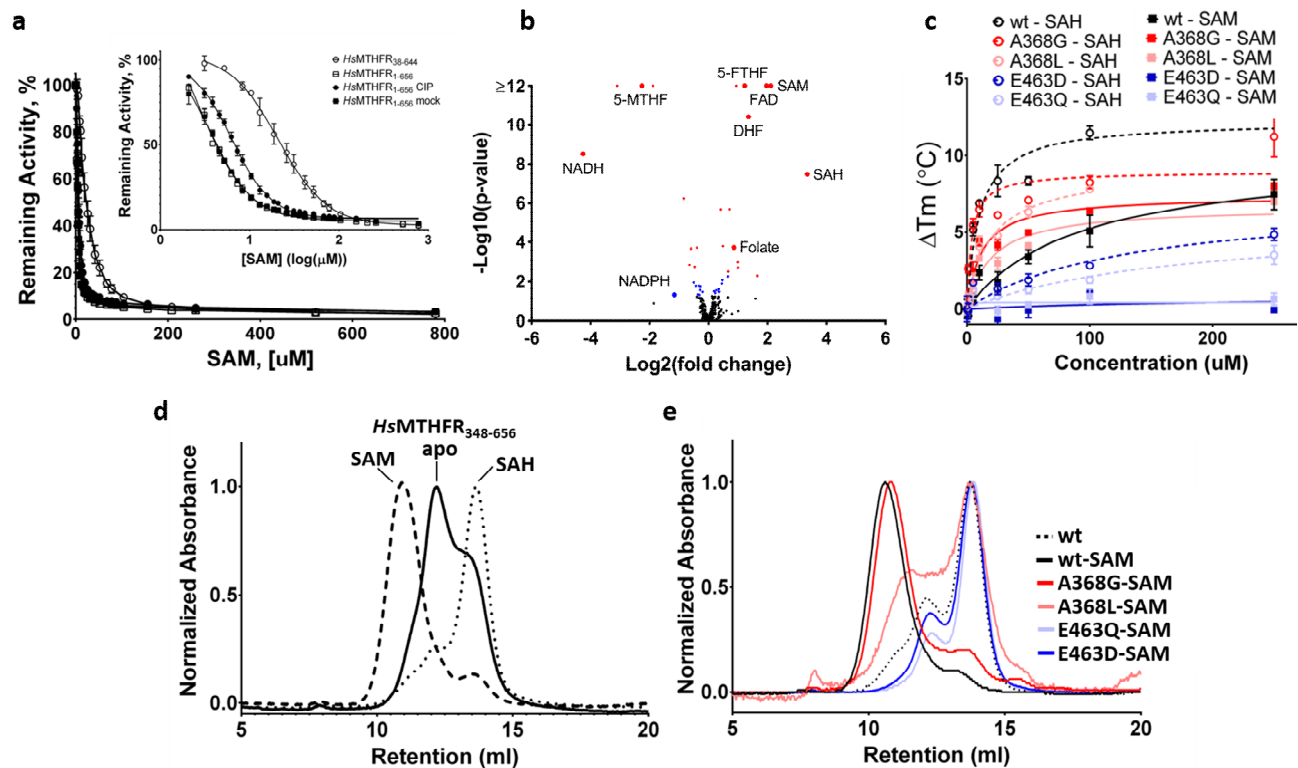


Fig. 3 Biophysical characterisation of hsMTHFR. (a) Inhibition of MTHFR catalytic activity following pre-incubation with various concentrations of SAM. Inset shows a replot transformed by log₁₀. (b) hsMTHFR-metabolite interactions revealed by MIDAS. Two-tiered significance cut-off: (•) $p < 0.05$; (◐) $p < 0.05$, $q < 0.1$. Known MTHFR-interacting metabolites are labeled. (c) DSF of hsMTHFR₃₄₈₋₆₅₆ protein wild-type or variant proteins incubated with increasing concentrations of SAH/SAM. (d) Size exclusion chromatography of hsMTHFR₃₄₈₋₆₅₆ incubated with SAM, SAH, or buffer (apo). (e) Size exclusion chromatography of hsMTHFR₃₄₈₋₆₅₆ wild-type or variant proteins pre-incubated with SAM.

Protein-metabolite interactions revealed by mass spectrometry

In collaboration with the Rutter's group (University of Utah), we mapped the metabolite interactome of hSMTHFR₃₈₋₆₄₄ using a mass spectrometry-based equilibrium dialysis approach ('MIDAS') that exhibits sensitivity up to 2 mM ligand affinities (22). Furthermore, MIDAS can reveal both non-catalytic and catalytic metabolite interactions as positive or negative fold change, respectively. Screening through a library of 412 human metabolites, we detected the known interactions of MTHFR including substrate (5-MTHF), substrate analog (folate), co-factors (NAD(P)H and FAD), allosteric regulators (SAM and SAH), and inhibitors (5-FTHF and DHF) (**Fig. 3b**), confirming the functional integrity of our protein. We also found that the regulatory domain alone construct hSMTHFR₃₄₈₋₆₅₆ is sufficient for the interactions with SAM and SAH as detected by MIDAS.

Differential scanning fluorimetry and size exclusion chromatography

Binding of the allosteric inhibitor SAM has previously been attributed to the MTHFR regulatory domain (2). We have demonstrated that the regulatory domain alone (hSMTHFR₃₄₈₋₆₅₆) is sufficient to bind SAM and SAH, through dose-dependent increases in thermostability by differential scanning fluorimetry (DSF) when exposed to increasing concentrations of each ligand (**Fig. 3c**). This confirms that the regulatory domain is a SAM/SAH binding module.

We have also employed analytical size exclusion chromatography (aSEC) to study the solution behaviour of MTHFR regulatory domain in response to SAM/SAH binding. Exposure of MTHFR₃₄₈₋₆₅₆ to SAM and SAH resulted in a leftward and rightward shift, respectively, of elution volume (V_e) compared to as-purified apo-protein (**Fig. 3d**). We interpret this to mean that binding of SAM and SAH to the MTHFR regulatory domain elicits significant, yet different, changes to the domain conformation.

Structural Data

Overall structure

We have determined the 2.5 Å resolution structure of hSMTHFR₃₈₋₆₄₄ in complex with FAD and SAH by Se-MAD. The hSMTHFR₃₈₋₆₄₄ protomer (**Fig. 4a**) is an overall elongated molecule comprised of the N-terminal catalytic domain (residues 40-337) and C-terminal regulatory domain (residues 363-644). The two domains do not contact each other directly but are connected by an extended linker (residues 338-362) traversing twice between the two domains. The hSMTHFR₃₈₋₆₄₄ structure reveals a homodimer (**Fig. 4b**), consistent with native mass spectrometry and small angle x-ray scattering. Dimerisation is mediated almost entirely by the regulatory domain such that the two catalytic domains are presented away from the dimeric interface and at opposite ends of the overall shape.

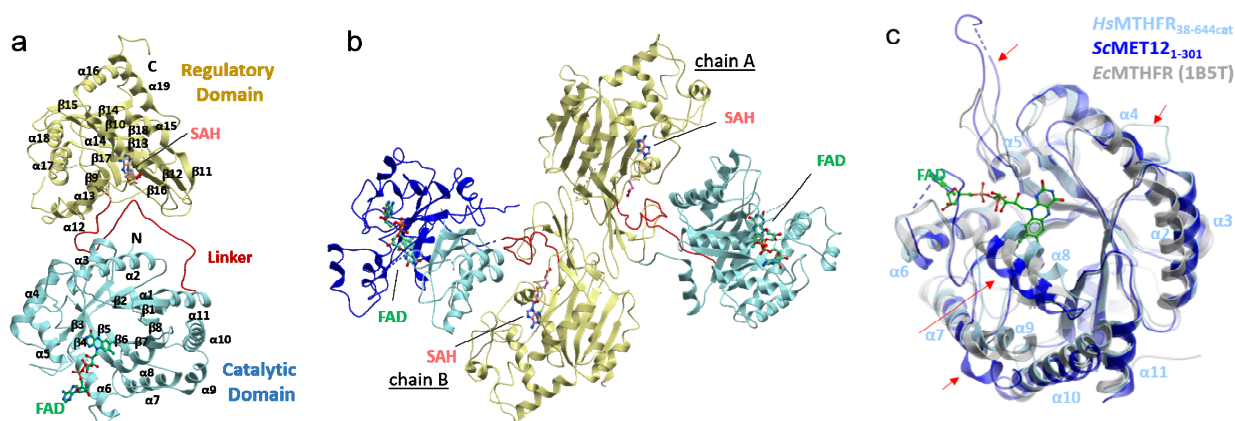


Fig. 4 Structure of hSMTHFR₃₈₋₆₄₄. (a) Topology of a monomer hSMTHFR showing catalytic domain (cyan), linker (red) and regulatory domain (yellow). Bound FAD (green) and SAM (pink) are shown in sticks. (b) Homodimer architecture of hSMTHFR is shown with the same colour scheme as panel a. (c) Structural alignment of hSMTHFR₃₈₋₆₄₄ (cyan) with *E. coli* (grey) and yeast (blue) orthologues. Four sites of important structural differences are indicated by arrows.

Evolutionary conservation of catalytic TIM-barrel

The N-terminal catalytic domain, bound with FAD cofactor in our structure, adopts the TIM-barrel structure evolutionarily conserved across all kingdoms. In addition to hsMTHFR₃₈₋₆₄₄ we also determined the catalytic domain structure of the yeast homolog MET12 (scMET12₁₋₃₀₁) to 1.56 Å resolution. This enables a structural comparison of the catalytic features across mammalian (hsMTHFR₃₈₋₆₄₄ structure), low-eukaryotic (scMET12₁₋₃₀₁ structure) and bacterial (previous structures from *E. coli*, *H. influenzae*, *T. thermophilus*) orthologues (**Fig. 4c**). Consistent with their sequence conservation, the catalytic domains have highly superimposable folds (main chain RMSD: 1.85 Å) with small local structural differences. The human enzyme has largely preserved the FAD binding site from lower organisms. In the absence of NADPH-bound complexes for hsMTHFR and scMET12 it remains unclear how eukaryotic enzymes preferentially use NADPH, compared to NADH for prokaryotes.

Regulatory domain is a novel SAM-binding fold

The C-terminal regulatory domain is unique among eukaryotic MTHFR. The core of this fold comprises two mixed β-sheets of 5 strands each interspersed with three loop extensions containing α-helices. To our knowledge the hsMTHFR regulatory domain represents a unique SAM binding architecture distinct from the 18 known classes of SAM-dependent methyltransferases and non-methyltransferases (23). Further, we found no annotations of this domain through our searches of the DALI/PFAM/CATH/SCOP servers.

Chemical Matter

In our hsMTHFR structure, the regulatory domain is bound with the SAM analogue, SAH. This is consistent with native mass spectrometry data showing that each dimer of as-purified hsMTHFR₃₈₋₆₄₄ was found to be bound with 0, 1 or 2 units of SAH. SAH is bound in an extended conformation in a pocket formed partly by the regulatory domain, and partly by the extensive inter-domain linker (**Fig. 5a**). We identified two conserved residues, Glu463 and Ala368, which are key to ligand binding. Glu463 forms a hydrogen bond with a ribose hydroxyl group from the SAH adenosyl moiety, while Ala368 is in close contact (3.7 Å) with the homocysteine sulfur atom. The native ligand for the regulatory domain, namely the methylated form SAM, is expected to bind to the same site and in a similar configuration as SAH. Notably, the additional methyl group in the sulphonium centre of SAM would create a steric clash to the Ala368 position depicted in the SAH-bound structure (**Fig. 5b**). Therefore, SAM binding likely results in conformational rearrangement of the loop region containing Ala368 to accommodate its methyl moiety.

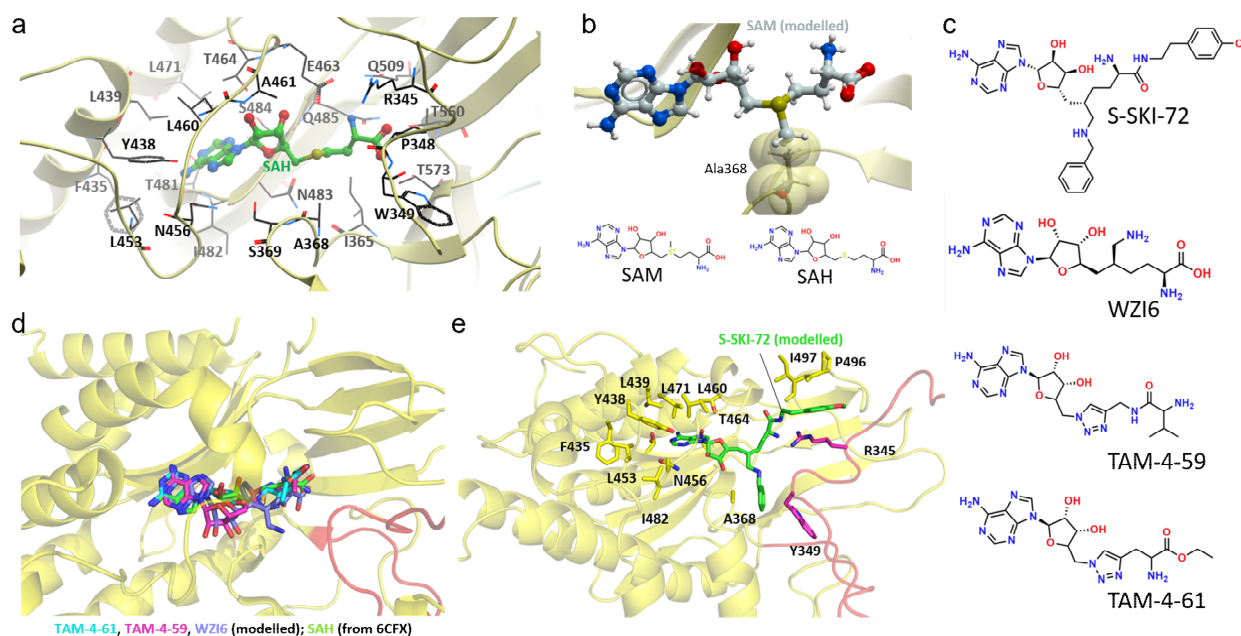


Fig. 5 Ligand binding to hsMTHFR regulatory domain. (a) Binding of SAH to regulatory domain revealed from hsMTHFR₃₈₋₆₄₄ crystal structure. (b) Schematic showing potential steric clash between modelled SAM and Ala368 of hsMTHFR₃₈₋₆₄₄. Bottom panel shows chemical structures of SAM and SAH. (c) Chemical structures of the 4 SAM analogues shown to bind hsMTHFR regulatory domain from DSF screening. (d) Virtual docking model of TAM-4-61 (cyan), TAM-4-59

(magenta) and WZI6 (blue) to regulatory domain overlaid with SAH (green) from the experimental structure of hsMTHFR₃₈₋₆₄₄. **(e)** Virtual docking model of (S)-SKI-72 with hsMTHFR regulatory domain.

IMPORTANT: Please note that the existence of small molecules within this TEP indicates only that chemical matter might bind to the protein in potentially functionally relevant locations. The small molecule ligands are intended to be used as the basis for future chemistry optimisation to increase potency and selectivity and yield a chemical probe or lead series. As such, the molecules within this TEP should not be used as tools for functional studies of the protein as they are not sufficiently potent or well-characterised to be used in cellular studies.

To confirm the roles of Ala368 and Glu463, we carried out DSF and aSEC assays (described above) on site-directed variants. The E463D and E463Q variants, aimed at abolishing key SAM-binding interactions, result in hsMTHFR₃₄₈₋₆₅₆ protein that no longer binds SAM (DSF, **Fig. 3c**) nor changes conformation in its presence (aSEC, **Fig. 3e**). The A368L variant, introducing a bulky side-chain in proximity to the SAM sulphonium centre, results in hsMTHFR₃₄₈₋₆₅₆ protein that retains the ability to bind SAM (**Fig. 3c**) but is less sensitive to change conformation in its presence (**Fig. 3e**). From these experiments we conclude that Glu463 is crucial to SAM binding, and Ala368 to SAM sensing.

Since the regulatory domain alone is sufficient to bind SAM and SAH, we screened a library of 162 SAM mimetics against hsMTHFR₃₄₈₋₆₅₆ using DSF, and have identified 4 hits (**Fig. 5c**) exhibiting increase in thermostability of 11 °C ((S)-SKI-72), 4 °C (WZI-6), 2.7 °C (TAM-4-59) and 2.7 °C (TAM-4-61), respectively. While three of them (WZI-6, TAM-4-59, and TAM-4-61) are close analogues of sinefungin, (S)-SKI-72 was recently developed at the SGC as a potent cellular probe of coactivator associated arginine methyltransferase 1 (CARM1, also known as PRMT4).

We performed virtual docking of the four ligand hits onto the regulatory domain of our hsMTHFR structure (PDB code 6FCX). The three sinefungin analogues WZI6, TAM-4-59 and TAM-4-61 dock to the same binding site in very similar configurations as SAM and SAH, as expected due to their structural similarity (**Fig. 5d**). The (S)-SKI-72 adenine moiety can occupy the same pocket as the SAH adenine moiety whilst its phenyl group is accommodated between Ala368 from the regulatory domain and Trp349 of the linker region (**Fig. 5e**). Similarly, the second methyl group of (S)-SKI-72 is located between the regulatory domain (Pro496 and Ile497) and the linker regions of MTHFR, interacting with the aliphatic side chain of Arg345 (**Fig. 5e**). The interaction between S-SKI-72 and the linker region of MTHFR indicates that binding of this molecule likely exerts conformational change on MTHFR. Comparison of the experimental structure of PRMT4 bound to (S)-SKI-72 (PDB code 6D2L) with our virtual docking model suggests (S)-SKI-72 to adopt a different conformation in MTHFR, as there is no structural similarity between the PRMT4 and MTHFR binding pockets.

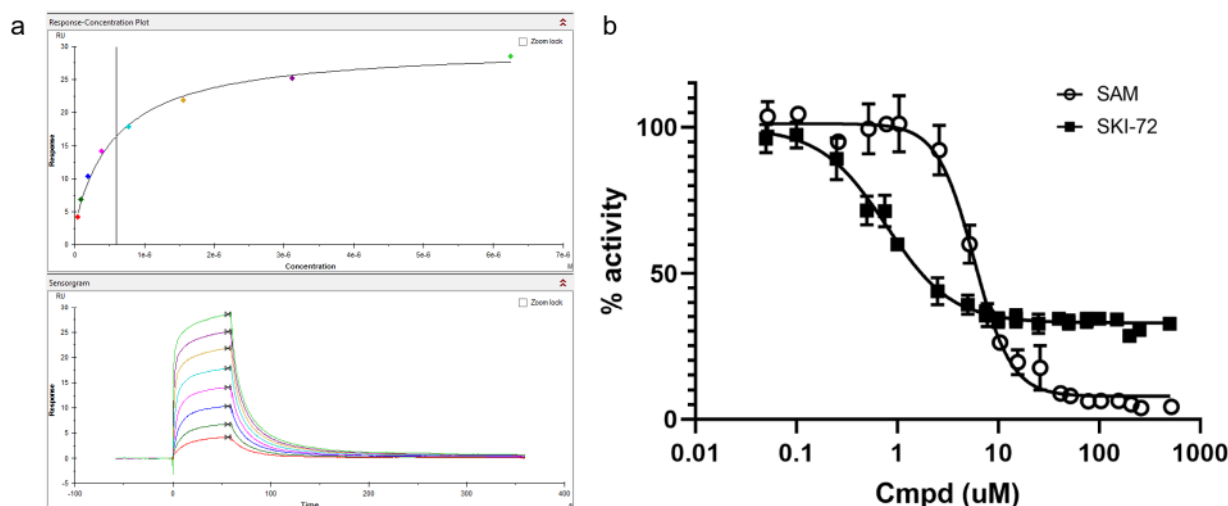


Fig. 6 Solution characterization of (S)-SKI-72 binding and inhibition of MTHFR. **(a)** SPR experiment of hsMTHFR₃₈₋₆₄₄ immobilized onto a CM5 sensor in the presence of increasing concentrations of (S)-SKI-72, showing steady-state analysis

(top) and sensorgram (bottom). (b) Inhibition kinetics of hsMTHFR activity in the presence of (S)-SKI-72 and SAM plotted as log(inhibitor) vs response.

We applied the surface plasmon resonance (SPR) method to validate solution binding of (S)-SKI-72 to hsMTHFR in the context of full-length protein, showing that it binds to immobilized hsMTHFR₃₈₋₆₄₄ with sub-micromolar affinity (K_d 596 nM and 612 nM in $n=2$ experiments)(Fig. 6a). Using SPR, we also validated our DSF data that indicated the regulatory domain is sufficient for (S)-SKI-72 binding (K_d 1.47 μ M and 1.175 μ M for hsMTHFR₃₄₈₋₆₅₆, in $n=2$ experiments), exhibiting similar affinity as SAM (K_d 1 μ M). Additionally, assay of hsMTHFR enzymatic activity in the presence of (S)-SKI-72 identifies it to be a more potent inhibitor than SAM (K_i of 0.8 μ M vs 3 μ M). However, unlike SAM, (S)-SKI-72 is unable to fully inhibit MTHFR, even at high concentrations (>100 μ M)(Fig. 6b). Altogether our data suggest derivatization of (S)-SKI-72 to be a promising route for the generation of potent, selective, inhibitors of MTHFR.

CONCLUSION

This TEP reveals the first structural view of a eukaryotic MTHFR enzyme, which is distinguished from its bacterial counterparts through having evolved regulatory modules for its own phosphorylation at multiple sites and allosteric inhibition of activity by SAM. Our data points to the phosphorylation of MTHFR at its N-terminus as a means to modulate the sensitivity towards inhibition of its activity by SAM that takes place at the C-terminus, through an extensive linker that functionally connects these regions and transmits a ligand-bound signal from the regulatory to the catalytic domain.

Modulating the finite control of MTHFR towards the level of such a key metabolite as SAM may be of pharmacological interest, including in cancer metabolism (13,16). Small molecules targeting MTHFR will help to elucidate its role in determining the flow of one-carbon units from folate cycle to the methionine cycle. This will impact our understanding of rare diseases in which enzymatic function in one of these pathways is missing, as well as in cancer, where upregulation of the folate/methionine cycles and one-carbon unit availability is increasingly understood to be a driving agent of disease.

Since MTHFR harbours a unique fold for binding SAM allosterically, this can be exploited to develop selective compounds that do not affect other SAM-binding proteins. We are currently following up the validation of SAM-analogues identified here to bind MTHFR whilst independently pursuing a collaboration for high-throughput screening (through the DNA-encoded library platform, X-CHEM). We rationalise that small molecules have the potential to lock MTHFR in the “inhibited” (as with SAM binding) or “dis-inhibited” (as with SAH binding) state.

Screening against a library of SAM/SAH analogues identified (S)-SKI-72 to bind MTHFR through its regulatory domain with high affinity. Medicinal chemistry efforts are currently being pursued in collaboration with Dr. Minkui Luo (Memorial Sloan Kettering Cancer Center), to create a new generation of (S)-SKI-72 derivatives that are more selective for MTHFR. Synthesis of analogues will focus on exploration of several substructures off the (S)-SKI-72 chemical backbone, to determine structure-activity relationships.

The two-domain architecture of MTHFR implies that SAM mediates its inhibitory effect through a long-range conformational change, to transmit the SAM-bound signal from the regulatory domain to the catalytic core through the extensive inter-domain linker. The outcome of the signal transduction event could be occlusion of the active site, thereby inhibiting MTHFR activity. Our data to date suggest that while (S)-SKI-72 could interact extensively with MTHFR through the regulatory domain, the underlying conformational change may not reach the same extent as does AdoMet, due to subtle differences in the binding modes between (S)-SKI-72 and SAM. This would explain why (S)-SKI-72 did not inhibit MTHFR fully. Future investigation of conformational flexibility and protein dynamics by experimental (e.g. cryo-electron microscopy) and computational (molecular dynamics simulation) approaches are underway.

This TEP further provides the starting point and tools for further characterisation of MTHFR functions, for instance, more precise mechanistic studies towards the identification of kinase(s) responsible for MTHFR phosphorylation *in vivo* (with the potential to desensitise MTHFR to SAM-mediated inhibition). Additionally, different structural methods can be employed in combination to delineate conformational changes of the entire protein as well as the molecular basis of MTHFR specificity for NADPH.

FUNDING INFORMATION

The work performed at the SGC has been funded by a grant from Wellcome [106169/ZZ14/Z].

ADDITIONAL INFORMATION

Structure Files

PDB ID	Structure Details
6CFX	Structure of hsMTHFR in complex with FAD and SAH
6FNU	Structure of scMET12 catalytic domain

Non-SGC resources

Commercially available CRISPR/Cas9 knockout plasmids
SCBT: Cat # sc-406554-KO-2
Genscript: Cat # 4524 These sgRNA sequences were validated in Sanjana N.E., Shalem O., Zhang F. Improved vectors and genome-wide libraries for CRISPR screening . Nat Methods. 2014, 11(8):783-4.
Commercially available antibodies
Thermofisher: MA5-15844 (monoclonal)
SCBT: x sc-517229 (monoclonal)

Materials and Methods

Protein Expression and Purification

*hsMTHFR*₁₋₆₅₆ and *hsMTHFR*₃₈₋₆₄₄

SGC ID: MTHFRA-c034 ([hsMTHFR](#)₁₋₆₅₆), MTHFRA-c042 ([hsMTHFR](#)₃₈₋₆₄₄)

Vector: pFB-CT10HF-LIC

Entry clone accession: BC053509

Cell line: DH10Bac

Tags and additions: C-terminal, TEV protease cleavable deca-histidine tag

Construct protein sequence of MTHFRA-c034 ([hsMTHFR](#)₁₋₆₅₆):

MVNEARGNSSLNPCLEGSASSGSESSKSSRCSTPGLDPERHERLREKMRRRLES GDKWFSLEFFPPRTAEGAVNLISRFDR
MAAGGPLYIDVTWHPAGDPGSDKETSSMMIASTAVNYCGLETILHMTCCRQRLEEITGHLHKAKQLGLKNIMALRGDPIGD
QWEEEGGFNYAVDLVKHIRSEFGDYFDICVAGYPKGHPEAGSFEADLHLKEKVSAGADFIITQLFFEADTFFRFVKA
GDMGITCPIVPGIFPIQGYHSLRQLVKLSKLEVPQEIKDVIPIKDNDAIRNYGIELAVSLCQELLASGLVPGLHFYTLNRE
MATTEVLKRLGMWTEDP RRPLWALSHPKRREEDVRPIFWASRPKSIYRTQEWDEFNPNRWRGNSSSPAFGELKDY
YLFYLSKSPKE ELLKMWGEELTSEASVFEVFLYLSGEPNRRNGHKVTCPLWNDEPLAAETSLLELLRVNRQ
GILTINSQPNINGKPSSDPIVGGWPSGGYVFQKAYLEFFTSRETAEALLQVLKYLVRVNYHLVNVKGENITNAPE
LQPNVAVTWGIFPGREIIQPTVVDPVSFMMWKDEAFALWIEQWGKLYEESPSRTIIQYIHDNYFLVNLVDNDFPL
DNCLWQVVEDTLELLNRPTQNARETEAPAENLYFQ_*
SHHHHHHHHHHDYKDDDDK

Construct protein sequence of MTHFRA-c042 ([hsMTHFR](#)₃₈₋₆₄₄):

MDPERHERLREKMRRRLES GDKWFSLEFFPPRTAEGAVNLISRFDRMAAGGPLYIDVTWHPAGDPGSDKETSSMMIA
STAVNYCGLETILHMTCCRQRLEEITGHLHKAKQLGLKNIMALRGDPIGDQWEEEGGFNYAVDLVKHIRSEFGDY
FDICVAGYKGHPEAGSFEADLHLKEKVSAGADFIITQLFFEADTFFRFVKA GDMGITCPIVPGIFPIQGYHSLR
QLVKLSKLEVPQEIKDVIPIKDNDAIRNYGIELAVSLCQELLASGLVPGLHFYTLNREMATTEVLKRLGMWTE
DP RRPLWALSHPKRREEDVRPIFWASRPKSIYRTQEWDEFNPNRWRGNSSSPAFGELKDY YLFYLSKSPKE
ELLKMWGEELTSEASVFEVFLYLSGEPNRRNGHKVTCPLWNDEPLAAETSLLELLRVNRQ GILTINSQP
NINGKPSSDPIVGGWPSGGYVFQKAYLEFFTSRETAEALLQVLKYLVRVNYHLVNVKGENITNAPELQPN
VAVTWGIFPGREIIQPTVVDPVSFMMWKDEAFALWIEQWGKLYEESPSRTIIQYIHDNYFLVNLVDNDFPL
DNCLWQVVEDTLELLNAENLYFQ_*
SHHHHHHHHHHDYKDDDDK

(underlined sequence contains vector encoded His-tag and TEV protease cleavage site*)

Bacmid DNA was prepared from DH10Bac cells and using to transfect Sf9 insect cells for the preparation of initial baculovirus. MTHFR protein was expressed from infected Sf9 cells cultivated in InsectXpress medium (Lonza) for 72 hours at 27°C.

Harvested cells were resuspended in lysis buffer (50 mM HEPES pH 7.5, 500 mM NaCl, 5% Glycerol, 20 mM Imidazole pH 7.5, 0.5 mM TCEP, 1 µL per 1 mL protease inhibitor cocktail EDTA-free).

Cell pellet was dissolved in approximately 200 mL lysis buffer and broken by sonication, done at 35% amplitude for 5 minutes with cycles of 5 seconds on and 10 seconds off. The cell debris was pelleted at 35000 x g, 1h and the supernatant used for purification with Nickel resin.

Buffers used:

Binding Buffer: 50 mM HEPES pH 7.5, 500 mM NaCl, 5% Glycerol, 20 mM Imidazole pH 7.5, 0.5 mM TCEP

Wash Buffer: 50 mM HEPES pH 7.5, 500 mM NaCl, 5% Glycerol, 40 mM Imidazole pH 7.5, 0.5 mM TCEP

Elution Buffer: 50 mM HEPES pH 7.5, 500 mM NaCl, 5% Glycerol, 250 mM Imidazole pH 7.5, 0.5 mM TCEP

The clarified cell extract was added to 5 ml of Ni-NTA resin pre-equilibrated with lysis buffer and passed through a glass column. The column was then washed with Binding Buffer (2 x 50 mL) and Wash Buffer (2 x 50 mL). The protein was eluted with Elution Buffer in 5 x 5 mL fractions. The eluted fractions from column 1 were pooled and concentrated to 10 mL with a 50 kDa MWCO spin concentrator and injected into an S200 16/60 column (pre-equilibrated in GF Buffer (50 mM HEPES pH 7.5, 500 mM NaCl, 0.5 mM TCEP, 5% Glycerol)) at 1.0 mL/min. 1.5 mL-fractions were collected. The eluted protein was pooled and concentrated to 17 mg/mL using a 50 kDa MWCO concentrator.

Regulatory Domain (hsMTHFR₃₄₈₋₆₅₆)

SGC ID: MTHFRA-c113

Vector: pNIC28-Bsa4

Entry clone accession: BC053509

Cell line: *E. coli Rosetta*

Tags and additions: N-terminal, TEV protease cleavable hexa-histidine tag

Construct protein sequence:

MHHHHHSSGVDLGTENLYFQ*SMPWALSAHPKRREEDVRPIFWASRPKSYIYRTQEWDEFNPNRWRWGNSSSPAFGELKD
YYLFYLKSKSPKEELLKMWGEELTSEASVFEVFLVYLSGEPNRNGHKVTCLPWNDEPLAAETSLKELLRVNRQGILTINSQPN
INGKPSSDPIVWGWPSSGGYVFQKAYLEFFTSRETAEALLQVLKKEYLRVNYHLVNVKGENITNAPELQPNNAVTVWGFIPGREIIQ
PTVVDPVFSFMFWKDEAFALWIEQWGLYEEESPSRTIIQYIHDNYFLVNLVDNDFPLDNCLWQVVEDTLELLNRPTQNARET
EAP

(underlined sequence contains vector encoded His-tag and TEV protease cleavage site*)

DNA was transformed into BL21(DE3) cells, plated and then used to inoculate a small-scale LB culture. This was then used to inoculate 6L of TB media. Cultures were induced overnight at 18°C with 0.1mM IPTG.

Harvested cells were resuspended in lysis buffer (50 mM HEPES pH 7.5, 500 mM NaCl, 5% Glycerol, 20 mM Imidazole pH 7.5, 0.5 mM TCEP, 1 µL per 1 mL protease inhibitor cocktail EDTA-free).

The cell pellet was dissolved in approximately 200 mL lysis buffer and broken by sonication, performed at 35% amplitude for 5 minutes with cycles of 5 seconds on and 10 seconds off. The cell debris was pelleted at 35000 x g, 1h and the supernatant used for purification with Nickel resin.

Buffers used:

Binding Buffer: 50 mM HEPES pH 7.5, 500 mM NaCl, 5% Glycerol, 20 mM Imidazole pH 7.5, 0.5 mM TCEP

Wash Buffer: 50 mM HEPES pH 7.5, 500 mM NaCl, 5% Glycerol, 40 mM Imidazole pH 7.5, 0.5 mM TCEP

Elution Buffer: 50 mM HEPES pH 7.5, 500 mM NaCl, 5% Glycerol, 250 mM Imidazole pH 7.5, 0.5 mM TCEP

The clarified cell extract was added to 5 ml of Ni-NTA resin pre-equilibrated with lysis buffer and passed through a glass column. The column was then washed with Binding Buffer (2 x 50 mL) and Wash Buffer (2 x 50 mL). The protein was eluted with Elution Buffer in 5 x 5 mL fractions. The eluted fractions from column 1 were pooled and concentrated to 10 mL with a 30 kDa MWCO spin concentrator and injected into an S200 16/60 column pre-equilibrated in GF Buffer (50 mM HEPES pH 7.5, 500 mM NaCl, 0.5 mM TCEP, 5% Glycerol) at 1.0

mL/min. 1.5 mL-fractions were collected. The eluted protein was pooled and concentrated to 17 mg/mL using a 30 kDa MWCO concentrator.

Assays

All enzymatic assays were performed using the physiological forward assay described by Suormala et al (21) with modifications as described by Rummel et al (24) and Burda et al (11,25). Only minor adaptations were made for use with pure recombinant protein, including reducing the assay time to 7 minutes and the addition of BSA to keep purified proteins stable. For SAM inhibition, purified SAM (26) was used. The K_i was estimated following a plot of $\log(\text{inhibitor})$ vs. response and a four-parameter curve fit as performed by GraphPad Prism (v6.07).

Analytical gel filtration was performed on a Superdex 200 HiLoad 10/30 column (GE Healthcare) pre-equilibrated with 10 mM HEPES pH 7.5, 150 mM NaCl and 5% glycerol in the presence or absence of 250 μM SAH or SAM (both Sigma-Aldrich).

Differential scanning fluorimetry was used to assay shifts in melting temperature caused by ligand binding in a 96-well PCR plate using an LC480 light cycler (Roche). Each well (20 μl) consisted of protein (0.1 mg ml^{-1}), SYPRO-Orange (Invitrogen) diluted 1000X, and buffer (10 mM HEPES pH 7.5, 500 mM NaCl) in the presence of 0 - 250 μM SAM, SAH or analogue compounds.

Surface Plasmon Resonance (SPR)

SPR was used to determine the affinity between hSMTHFR₃₈₋₆₄₄ and (S)-SKI-72. 30 μg of hSMTHFR₃₈₋₆₄₄ was immobilised onto Sensor Chip CM5 sensor (series S) via the protein -NH₂ groups employing 1-Ethyl-3-(3-dimethylaminopropyl)carbodiimide crosslinker (EDC) and N-hydroxysuccinimide (NHS) in acetate buffer pH 4.0. For the binding experiment, (S)-SKI-72 was serially diluted from 6.25 μM to 0.05 μM in 20 mM Hepes pH 7.5, 150 mM NaCl, 0.5 mM TCEP, 0.05% Tween, 5% DMSO. Association and dissociation times were set for 60 seconds and 90 seconds, respectively. Data were analysed using the Biacore S200 Evaluation Software.

Mass spectrometry

Mass spectrometry of hSMTHFR proteins under native conditions was performed on an Agilent 1290 uHPLC system, in accordance with previously published protocol (27).

To prepare samples for phosphorylation mapping, 20-100 μg hSMTHFR₁₋₆₅₆ was reduced in 100 μl of 100 mM ammonium bicarbonate buffer, pH 7.5 by addition of 1 μl of 1 M DTT and incubation at 56°C for 40 minutes. Alkylation was performed by addition of 4 μl of saturated iodoacetamide solution and incubated at room temperature in the dark for 20 minutes. Endoprotease digestion was performed using either trypsin, *Smart Digest* trypsin (Thermo) or pepsin. LC-MSMS analyses were performed using both whole endoprotease digests and metal oxide affinity enriched samples, on a Dionex U3000 nanoHPLC coupled to a Bruker Esquire HCT ion trap mass spectrometer.

Crystallisation & Structure Determination

Proteins were concentrated to 15-20 mg/ml prior to crystallisation. hSMTHFR₃₈₋₆₄₄ crystals were grown by sitting drop vapour diffusion at 20°C, in mother liquor containing 0.1 M Na citrate tribasic, 22.5% PEG4K, 5% 2-propanol. scMET12₁₋₃₀₂ crystals were grown by sitting drop vapour diffusion at 20°C, in mother liquor containing 0.2M Na/K tartrate, 20% PEG3350. All crystals were cryo-protected in mother liquor containing ethylene glycol (25% v/v) and flash-cooled in liquid nitrogen.

X-ray diffraction data were collected at the Diamond Light Source and processed using XIA2 (28). The hSMTHFR₃₈₋₆₄₄ structure was solved by selenium multi-wavelength anomalous diffraction phasing using autoSHARP (29), and subjected to automated building with BUCCANEER (30). Phases for scMET12₁₋₃₀₂ were calculated by molecular replacement using the coordinates of *Thermus thermophilus* MTHFR (PDB code: 3APY) as model.

Ligand docking

To perform a virtual docking experiment employing the compounds identified in the DSF screen and hsMTHFR₃₈₋₆₄₄ (PDB code: [6FCX](#)) coordinates, we used ICM-Pro's standard docking algorithm and removed crystallographic SAH from MTHFR coordinates prior to docking. As a control, we docked SAH back into hsMTHFR model, which recapitulated the conformation observed in the crystal structure, suggesting that the modelled binding conformation of the compounds represent a good starting point for inferring their interactions with MTHFR.

References

1. Froese, D. S., Fowler, B., and Baumgartner, M. R. (2018) [Vitamin B12 , folate, and the methionine remethylation cycle-biochemistry, pathways, and regulation](#). *J Inherit Metab Dis*
2. Sumner, J., Jencks, D. A., Khani, S., and Matthews, R. G. (1986) [Photoaffinity labeling of methylenetetrahydrofolate reductase with 8-azido-S-adenosylmethionine](#). *J Biol Chem* **261**, 7697-7700
3. Yamada, K., Strahler, J. R., Andrews, P. C., and Matthews, R. G. (2005) [Regulation of human methylenetetrahydrofolate reductase by phosphorylation](#). *Proc Natl Acad Sci U S A* **102**, 10454-10459
4. Marini, N. J., Gin, J., Ziegler, J., Keho, K. H., Ginzinger, D., Gilbert, D. A., and Rine, J. (2008) [The prevalence of folate-remedial MTHFR enzyme variants in humans](#). *Proc Natl Acad Sci U S A* **105**, 8055-8060
5. Zhu, B., Xiahou, Z., Zhao, H., Peng, B., and Xu, X. (2014) [MTHFR promotes heterochromatin maintenance](#). *Biochem Biophys Res Commun* **447**, 702-706
6. Daubner, S. C., and Matthews, R. G. (1982) [Purification and properties of methylenetetrahydrofolate reductase from pig liver](#). *J Biol Chem* **257**, 140-145
7. Froese, D. S., Huemer, M., Suormala, T., Burda, P., Coelho, D., Gueant, J. L., Landolt, M. A., Kozich, V., Fowler, B., and Baumgartner, M. R. (2016) [Mutation Update and Review of Severe Methylenetetrahydrofolate Reductase Deficiency](#). *Hum Mutat* **37**, 427-438
8. Liew, S. C., and Gupta, E. D. (2015) [Methylenetetrahydrofolate reductase \(MTHFR\) C677T polymorphism: epidemiology, metabolism and the associated diseases](#). *Eur J Med Genet* **58**, 1-10
9. Frosst, P., Blom, H. J., Milos, R., Goyette, P., Sheppard, C. A., Matthews, R. G., Boers, G. J., den Heijer, M., Kluijtmans, L. A., van den Heuvel, L. P., and et al. (1995) [A candidate genetic risk factor for vascular disease: a common mutation in methylenetetrahydrofolate reductase](#). *Nat Genet* **10**, 111-113
10. Molloy, A. M., Daly, S., Mills, J. L., Kirke, P. N., Whitehead, A. S., Ramsbottom, D., Conley, M. R., Weir, D. G., and Scott, J. M. (1997) [Thermolabile variant of 5,10-methylenetetrahydrofolate reductase associated with low red-cell folates: implications for folate intake recommendations](#). *Lancet* **349**, 1591-1593
11. Burda, P., Schafer, A., Suormala, T., Rummel, T., Burer, C., Heuberger, D., Frapolli, M., Giunta, C., Sokolova, J., Vlaskova, H., Kozich, V., Koch, H. G., Fowler, B., Froese, D. S., and Baumgartner, M. R. (2015) [Insights into severe 5,10-methylenetetrahydrofolate reductase deficiency: molecular genetic and enzymatic characterization of 76 patients](#). *Hum Mutat* **36**, 611-621
12. Locasale, J. W. (2013) [Serine, glycine and one-carbon units: cancer metabolism in full circle](#). *Nat Rev Cancer* **13**, 572-583
13. Stankova, J., Lawrance, A. K., and Rozen, R. (2008) [Methylenetetrahydrofolate reductase \(MTHFR\): a novel target for cancer therapy](#). *Curr Pharm Des* **14**, 1143-1150
14. Lin, V. C., Lu, T. L., Yin, H. L., Yang, S. F., Lee, Y. C., Liu, C. C., Huang, C. Y., Yu, C. C., Chang, T. Y., Huang, S. P., and Bao, B. Y. (2016) [Prognostic Relevance of Methylenetetrahydrofolate Reductase Polymorphisms for Prostate Cancer](#). *Int J Mol Sci* **17**
15. Stankova, J., Shang, J., and Rozen, R. (2005) [Antisense inhibition of methylenetetrahydrofolate reductase reduces cancer cell survival in vitro and tumor growth in vivo](#). *Clin Cancer Res* **11**, 2047-2052

16. Sun, D. F., Weng, Y. R., Chen, Y. X., Lu, R., Wang, X., and Fang, J. Y. (2008) Knock-down of methylenetetrahydrofolate reductase reduces gastric cancer cell survival: an in vitro study. *Cell Biol Int* **32**, 879-887
17. Lawrance, A. K., Deng, L., and Rozen, R. (2009) Methylenetetrahydrofolate reductase deficiency and low dietary folate reduce tumorigenesis in *Apc min/+* mice. *Gut* **58**, 805-811
18. Chen, J., Gammon, M. D., Chan, W., Palomeque, C., Wetmur, J. G., Kabat, G. C., Teitelbaum, S. L., Britton, J. A., Terry, M. B., Neugut, A. I., and Santella, R. M. (2005) One-carbon metabolism, MTHFR polymorphisms, and risk of breast cancer. *Cancer Res* **65**, 1606-1614
19. Mentch, S. J., Mehrmohamadi, M., Huang, L., Liu, X., Gupta, D., Mattocks, D., Gomez Padilla, P., Ables, G., Bamman, M. M., Thalacker-Mercer, A. E., Nichenametla, S. N., and Locasale, J. W. (2015) Histone Methylation Dynamics and Gene Regulation Occur through the Sensing of One-Carbon Metabolism. *Cell Metab* **22**, 861-873
20. Mehrmohamadi, M., Mentch, L. K., Clark, A. G., and Locasale, J. W. (2016) Integrative modelling of tumour DNA methylation quantifies the contribution of metabolism. *Nat Commun* **7**, 13666
21. Suormala, T., Gamse, G., and Fowler, B. (2002) 5,10-Methylenetetrahydrofolate reductase (MTHFR) assay in the forward direction: residual activity in MTHFR deficiency. *Clin Chem* **48**, 835-843
22. Orsak, T., Smith, T. L., Eckert, D., Lindsley, J. E., Borges, C. R., and Rutter, J. (2012) Revealing the allosterome: systematic identification of metabolite-protein interactions. *Biochemistry* **51**, 225-232
23. Gana, R., Rao, S., Huang, H., Wu, C., and Vasudevan, S. (2013) Structural and functional studies of S-adenosyl-L-methionine binding proteins: a ligand-centric approach. *BMC Struct Biol* **13**, 6
24. Rummel, T., Suormala, T., Haberle, J., Koch, H. G., Berning, C., Perrett, D., and Fowler, B. (2007) Intermediate hyperhomocysteinaemia and compound heterozygosity for the common variant c.677C>T and a MTHFR gene mutation. *J Inherit Metab Dis* **30**, 401
25. Burda, P., Suormala, T., Heuberger, D., Schafer, A., Fowler, B., Froese, D. S., and Baumgartner, M. R. (2017) Functional characterization of missense mutations in severe methylenetetrahydrofolate reductase deficiency using a human expression system. *J Inherit Metab Dis* **40**, 297-306
26. Shapiro, S. K., and Ehninger, D. J. (1966) Methods for the analysis and preparation of adenosylmethionine and adenosylhomocysteine. *Anal Biochem* **15**, 323-333
27. Chalk, R. (2017) Mass Spectrometric Analysis of Proteins. in *Heterologous Gene Expression in E. coli: Methods and Protocols* (Burgess-Brown, N. A. ed.), Humana Press, New York. pp 373-396
28. Winter, G., Lobley, C. M., and Prince, S. M. (2013) Decision making in xia2. *Acta Crystallogr D Biol Crystallogr* **69**, 1260-1273
29. Vonrhein, C., Blanc, E., Roversi, P., and Bricogne, G. (2007) Automated structure solution with autoSHARP. *Methods Mol Biol* **364**, 215-230
30. Cowtan, K. (2006) The Buccaneer software for automated model building. 1. Tracing protein chains. *Acta Crystallogr D Biol Crystallogr* **62**, 1002-1011

We respectfully request that this document is cited using the DOI value as given above if the content is used in your work.